RADIATION RESEARCH 173, 536–544 (2010)
0033-7587/10 $15.00

DOI: 10.1667/RR1712.1

A Simple Quantitative Method for Assessing Pulmonary Damage after X Irradiation

L. Downing,[a] K. E. Sawarynski,[b] J. Li,[c] M. McGonagle,[d] M. D. Sims[a] and B. Marples[a,1]

[a] *Department of Radiation Oncology, William Beaumont Hospital, Royal Oak, Michigan 48073;* [b] *Infectious Diseases, William Beaumont Hospital, Royal Oak, Michigan 48073;* [c] *Department of Electrical and Computer Engineering, Oakland University, Rochester, Michigan 48309; and* [d] *Research Services, William Beaumont Research Institute, Royal Oak, Michigan 48073*

Downing, L., Sawarynski, K. E., Li, J., McGonagle, M., Sims, M. D. and Marples, B. A Simple Quantitative Method for Assessing Pulmonary Damage after X Irradiation. *Radiat. Res.* 173, 536–544 (2010).

Pulmonary damage after radiotherapy is typically characterized by an initial alveolar inflammation (pneumonitis) followed by chronic fibrosis. In the present study, changes in lung architecture were measured in the pneumonitis phase after whole-body low-dose X irradiation of C57BL/6 mice. Radiation damage was evaluated at 24 h and 1–8 weeks postirradiation. Three distinct scoring systems were used: (1) manually evaluating alveolar distortion and infiltration of inflammatory cells into the alveolar space using a continuous numerical scale across an entire lung section, (2) physically measuring the average thickness of the alveolar septa from multiple representative microscope fields, and (3) a new rapid automated mathematical algorithm based on image segmentation of alveolar space across an entire section. Each scoring method detected significant changes in alveolar architecture at the earliest times compared with sham-treated controls and gave comparable evaluations of injury. The results from the automated mathematical algorithm correlated significantly with both the manual evaluation method (Spearman's correlation coefficient $\rho = 0.044$) and the direct physical measurement of septa thickness ($\rho = 0.002$). These data demonstrate that evaluating alveolar space by segmentation analysis provides a reliable method for scoring early pulmonary radiation damage that is consistent with more established methodologies but is more rapid and is independent of potential operator and selection bias.

INTRODUCTION

The lung is a major dose-limiting organ for thoracic radiotherapy. The scale of radiation-induced injury is dependent on several factors including the total radiation dose, the specific treatment regimen, and the volume of lung irradiated (*1*). X irradiation of the lungs with high therapeutic doses can lead to early inflammatory pneumonitis (clinically evident during or soon after therapy) followed by latent fibrosis months after therapy due to the deposition of collagen (*2, 3*). Pneumonitis and fibrosis are a consequence of radiation damage to epithelial and endothelial parenchymal cells. These events lead to the activation of cytokine cascades and consequential infiltration of both recruited and local inflammatory cells into alveolar spaces (*4–9*). The pattern of chemokine production after thoracic irradiation differs substantially between the pneumonitic and fibrotic phases of injury (*10, 11*).

Typically, lung injury has been assessed by measuring changes in the architecture of tissue. Quantitative assessment scales have been developed for pulmonary injury in severe pathology such as asbestosis (*12*). However, such grading systems lack the necessary resolution to assess less severe or short-lived changes in tissue architecture such as that produced by low-dose radiation. To overcome this, simple qualitative grading scales have been devised that broadly categorize damage against a four-point scale (*13, 14*). Although functional, these qualitative scales can lack consistency between repeat assessments and can be prone to scoring bias. These limitations become more evident when damage is scored by different operators or when experiments extend over a number of years or between distant institutions.

Image analysis technology provides the best option to achieve consistent assessments of lung damage that are independent of individual operators. Moreover, automated approaches tend to be rapid and assess whole lung sections rather than a few representative histopathological fields selected randomly by a scorer bound by time constraints. This is particularly important when assessing pulmonary damage that is localized to specific structures. For example, damage from inhaled biological particles that produce localized bronchocentric injury would be underestimated if the number of randomly selected fields did not contain a representative quantity of bronchioles. Additionally, for the same reason, the

[1] Address for correspondence: Department of Radiation Oncology, William Beaumont Hospital, 3811 W. Thirteen Mile Rd., 105-RI, Royal Oak, MI 48073; e-mail: brian.marples@beaumont.edu.

extent of damage would also be underestimated if the experimental rationale was to examine the combined effects of two agents that produce different types of pulmonary damage confined to either the alveoli or bronchioles.

In this study we focused on scoring the initial phase of radiation-induced pulmonary damage during the first 8 weeks after low-dose exposure. Changes in pulmonary architecture and alveolar inflammation (pneumonitis) were evaluated. A comparative analysis was performed using two manual methods that assessed either the whole lung section or multiple randomly selected representative histological fields and a new automated mathematical approach using segmentation analysis developed specifically to score pulmonary injury. Our aim was to evaluate the stringency of the mathematical algorithm against the more established manual scoring techniques. The present study demonstrated that segmentation analysis of alveolar space from a standard hematoxylin and eosin (H&E)-stained digital image provided a simple but accurate measure of lung architecture that corresponded to a manual histopathology assessment of radiation-induced pulmonary damage. We conclude that this new rapid automated analysis methodology is both robust and free of operator bias.

MATERIALS AND METHODS

Animals

The experimental protocol was approved by the Institutional Animal Care and Use Committee of William Beaumont Hospital. Female C57BL/6 mice, 6–8 weeks old and approximately 20 g in weight, were purchased from Charles River Laboratories (Wilmington, MA) and housed in conventional microisolator cages to minimize pulmonary infections from external sources. Animals were allowed to acclimate from shipping for 1 week prior to treatment. Animals were given standard rodent chow and water *ad libitum*.

Radiation Schedule

Animals were whole-body irradiated at room temperature using a 160 kVp Faxitron X-ray machine (0.5-mm copper and aluminum filters). A dose of 2 Gy was given at a dose rate of 0.69 Gy/min. The mice were not anesthetized and remained unrestrained but confined in a plexiglass irradiation device to maintain posture and maximize dose homogeneity within the radiation beam (10 cm diameter). Sham-treated animals (0 Gy) were exposed to the same procedures but the radiation beam was not switched on. X-ray dosimetry was performed in collaboration with Dr. Elwood Armour at Johns Hopkins University (Baltimore, MD). A mouse phantom was used along with EBT-GAFChromic film for calibration. This technique was devised by Dr. Armour and provides a better dosimetry analysis for the experimental setup than can be achieved by an ionization chamber. To get maximum depth penetration, the Faxitron beam was filtered and used with a long source-to-skin distance. Copper filtration was supplied by Faxitron. After irradiation, the mice were returned to standard filter-top caging.

Tissue Isolation

Mice were killed humanely at 24 h or 1, 2, 4 or 8 weeks after irradiation, along with age-matched controls. Each study group contained five animals. Animals were anesthetized by i.p. injection of 0.1 ml sodium pentobarbital (1:9 mixture of Nembutal® and heparin at a dose of 50 mg/kg) and the chest cavity was opened with a midline incision to expose the lungs. Prior to lung removal, a tracheotomy was performed to inflate the lungs by perfusion with 1 ml neutral buffered formalin and the aorta was surgically tied off to keep the lungs inflated. The inflated lungs were removed from the thoracic cavity, fixed in formalin overnight at 4°C, and then placed in individual tissue cassettes in the same orientation, embedded in paraffin, cut along the longitudinal axis, and processed for histopathology staining.

Lung Pathology and Histology

Histological analysis was carried out on whole-lung sections prepared from formalin-fixed, paraffin-embedded tissues. Mounted paraffin sections (5 μm thick) were deparaffinized and rehydrated through graded ethanol and subsequently stained automatically with hematoxylin and eosin using a Thermo Scientific Microm HMS 740 Robotic Routine Stainer. Slides were deidentified and randomized and damage was assessed using each scoring method. Once all scoring and assessments were complete, the data were decoded to calculate the mean (± SEM) parameters for each method.

Assessment of Tissue Architecture using a Manual Four-Point Scale

The entire H&E-stained section was evaluated at low magnification (10× objective) and the level of damage was assessed using two parameters: (1) an estimate of the overall extent of infiltration of inflammatory cells into the alveolar spaces combined with (2) an evaluation of diffuse alveolar wall thickening and architectural deformation across the entire lung section. All inflammatory cells (neutrophils, macrophages, lymphocytes) were considered in the assessment of infiltration. The assessment of tissue deformation considered perivascular and peribronchiolar inflammation with destruction of bronchi and alveolae and hemorrhagic necrosis. The four-point scale of infiltration was: 0: no or occasional inflammatory cells; 1: few loosely arranged inflammatory cells; 2: many cells in intrastitial and intra-alveolar spaces; 3: numerous inflammatory cells in perivascular space. A general assessment of alveolar deformation was then made that considered progressive alveolar septal thickening and distortion, intrastitial and intra-alveolar edema, and hyperplasia of type II pneumocytes. The four-point scoring scale of alveoli deformation was: 0: normal appearance; 1: mild thickening (little distortion); 2: moderate thickening (increased distortion); 3: severe thickening (maximal distortion). The inflammatory assessment was then combined with the assessment of diffuse alveolar deformation to generate an overall definitive measure of tissue injury on a scale of 0–3. Examples of histological assessments made using these scales are shown in Fig. 1.

Assessment of Tissue Architecture by Physically Measuring Alveolar Septal Thickness

Alveolar wall thickness was measured in micrometers using the annotations and measurements length tool from the Nikon NIS-Elements image analysis program. This software tool required a high-powered microscope image to obtain accurate measurements, and therefore a 40× objective power was used. Multiple measurements were taken from 10 distinct histological fields selected randomly from the entire H&E-stained section for every animal in the group ($n = 5$). The average alveolar wall thickness was then calculated from 10 individual measurements per field by spanning the alveolar wall with the analysis tool and measuring wall thickness. Examples of changes in alveolar wall thickening with time postirradiation are shown in Fig. 2.

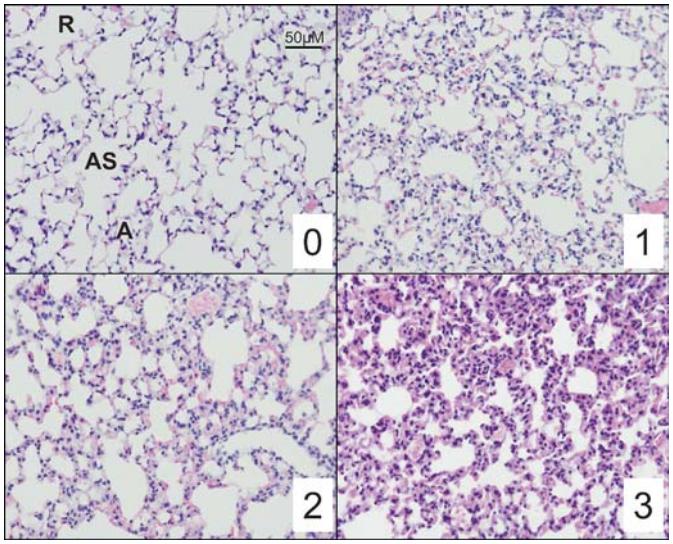

FIG. 1. Representative H&E-stained lung sections illustrating the four-point manual scoring scale. The lung sections are graded as (0) normal architecture with thin alveolar septa and distinct respiratory bronchioles (R), alveolar sacs (AR) and alveoli (A), (1) progressive thickening of alveolar septa and reduction of alveolar space, (2) diffuse increase in alveolar septal thickening and reduction in alveoli space with invasion of inflammatory cells, and (3) widespread loss of tissue architecture. Scale bar 50 μ*M*. Original magnification 200×.

Mathematical Assessment of Damage by Mathematical Segmentation Analysis

The algorithm was designed to capture information from a single digital feature of the entire H&E-stained section of the lung captured at low magnification (10× objective). The image was segmented to extract alveolar space and wall as regions of interests (ROI), and the numerical score was determined as the area ratio of alveolar wall as a product of the alveolar space. The segmentation process used pixel color as a discriminator since the pixels in the region of alveolar space have a very uniform color compared to those in the alveolar wall. This characteristic leads to a simple color-based pixel classification algorithm with five steps. Briefly, the image is converted from RGB color space to CIE L*a*b* color space (*15*). The three coordinates of the CIE L*a*b* color space are L*, a* and b*, where L* represents the lightness of the color, a* represents the position between red/magenta and green, and b* represents the position between yellow and blue. This color space removed the variations in pixel brightness. Only the information in a* and b* channels are used in the proceeding steps. The mean and variance of pixel color in the region of alveolar space was calculated and denoted C. Each pixel in the image was then classified according to its distance to C in the color space. If the distance was smaller than a threshold, the pixel is classified as a member of alveolar space. Otherwise, the pixel is classified as a member of alveolar wall. The output of classification is a binary image, where 0 represents an alveolar wall pixel and 1 represents an alveolar space pixel. A median filter is applied to the binary image to reduce misclassification and to generate the scoring parameter (R).

Statistical Analysis

Measured alveolar septal thickness was statistically evaluated by Student's *t* test assuming unequal variances, with *P* values less than 0.05 considered significant. The measured alveolar thickness, manual assessment of diffuse pulmonary damage (four-point scale) and the mathematical algorithm (segmentation analysis) were compared by Spearman's ρ correlation coefficient, a multivariate non-parametric measure of association. ρ values less than 0.05 were considered significant.

RESULTS

Radiation-induced changes in lung tissue architecture after a single whole-body dose of X radiation were evaluated over 8 weeks. Throughout the experiments no behavioral changes were observed in any of the treated animals and no animals exhibited physical symptoms of pulmonary distress.

Initially, a manual assessment of pulmonary injury was made using a qualitative scale defined by four broad categories. Typical examples of the 0–3 scoring scale are shown in Fig. 1. These typical images are from animals exposed to the same radiation dose but evaluated at different times postirradiation (score 0 from sham-treated control animal; score 1 from a 1-week postirra-

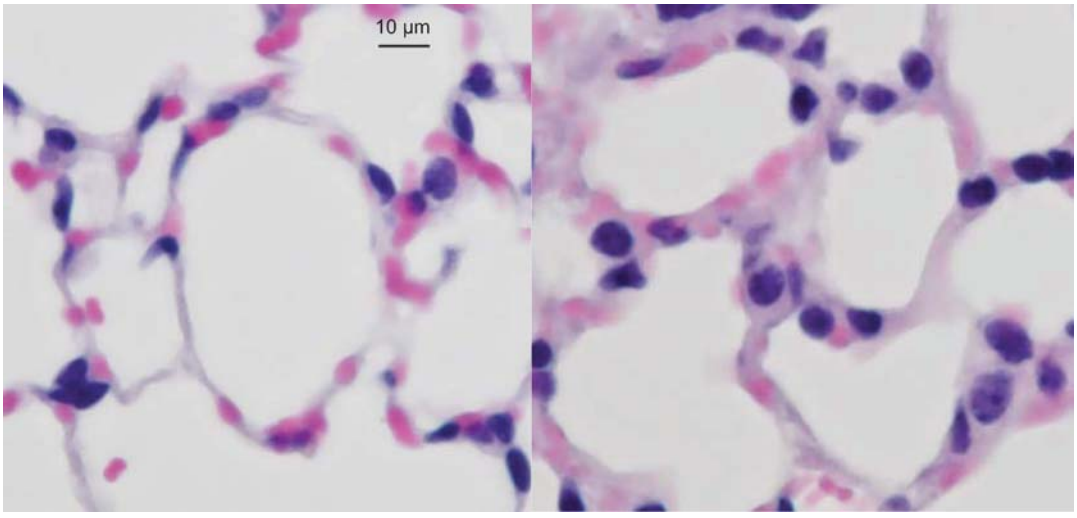

FIG. 2. Enlarged representative images showing changes in alveolar thickening after whole-body exposures to 2 Gy. Left: Sham-irradiated; right: 24 h postirradiation. Scale bar 10 μ*M*.

diation animal; scores 2 and 3 taken from two separate animals 24 h postirradiation). A score of zero was used to describe the typical lung structure of sham-treated animals or irradiated mice that exhibited only minimal damage over a small area of the lung. A numerical score of 3 was used to describe a highly distorted architecture with widespread alveolar thickening, invasion of inflammatory cells, and a large reduction in alveolar space.

Distinct respiratory bronchioles (R), alveolar sacs (AS) and single alveoli (A) can be seen in the histological sections evaluated with a zero score (Fig. 1). Pulmonary capillaries and vessels are also visible surrounding each alveolus. Adjacent alveoli are separated by a thin alveolar septum of flattened epithelial cells containing alveolar pores. Abundant type I and type II pneumocytes can be seen in the epithelium of the alveolar lining, the latter of which are widely regarded as cells critical in the radiation response. By contrast, there is a gross loss of structural architecture in tissue sections given a score of 3, and individual alveolar structures cannot be clearly identified. The diffuse thickening of the alveolar septa that is seen after radiation exposure is more evident at higher magnification (Fig. 2) and is associated with alveolar distortion and a reduction in the volume of the individual alveoli. Around individual bronchioles, interstitial and intra-alveolar edema contributes to the severity of the diffuse pattern of damage (Figs. 1 and 3). The alveolar space was reduced further in some cases by the invasion of resident and recruited inflammatory cells in the lung. Specific immunohistochemistry indicated the early invasion of neutrophils and lymphocytes followed by macrophages. The radiation-induced changes in lung tissue structure as a function of time after exposure defined by the four-point scale are shown in Fig. 4 (right panel). Although the highest assessment score was recorded at 24 h, the mean value was not significantly different from those obtained at other times. This lack of statistical significance can be attributed to the small group sizes, the variability in response between individual animals within each group, and the limitations of scoring using a four-point scale.

Next, the radiation-induced alveolar damage was quantified by assessing the change in thickness of alveolar septa from multiple measurements in 10 randomly selected microscope fields per animal ($n = 5$) at high magnification using Nikon NIS-Elements image analysis software (sample identifiers and treatments were blinded to the scorer). In sham-treated animals the mean septal wall thickness increased from 2.66 ± 0.27 μM to 3.84 ± 1.21 μM over the 8-week interval (Fig. 5). This increase was not statistically significant (Student's t test $P = 0.105$). In contrast, in radiation-exposed animals, a statistically significant thickening of the alveolar septum was evident 24 h after treatment (Student's t test $P = 0.029$) and remained statistically significant 2 weeks postirradiation ($P = 0.002$) compared with age-matched sham-treated animals (Fig. 5). At 4 ($P = 0.98$) and 8 ($P = 0.81$) weeks postirradiation, the thickening of the alveolar wall diminished and became statistically indistinguishable from that of age-matched sham-treated animals. These data demonstrate that radiation-induced changes in alveolar wall thickness occur as an early event after low-dose exposure.

The assessment of damage obtained by physically measuring alveolar septa thickness was then compared with that obtained using the manual four-point scale, since this latter approach is widely accepted as a standard method of damage assessment in the lung. Non-parametric multivariate analysis indicated a statistically significant positive correlation between the assessments made using two methods (Spearman's $\rho = 0.001$) (Fig. 6C).

Assessing the thickness of the alveolar wall is a time-consuming process and can take a number of hours per slide. Multiple individual measurements are needed in numerous randomly selected microscope fields to ensure a good degree of statistical robustness and to avoid inadvertent selection bias. Therefore, to improve the efficiency of assessing radiation-induced pulmonary damage and overcome concerns regarding selection bias, a mathematical algorithm was created to evaluate injury from a single low-magnification (10×) digital image of the entire lung section. The size of the alveolar space was extracted and defined as the region of interest (ROI), since this was the most homogeneous parameter. A simple digital mask was made on the alveolar space, such that the remaining image was regarded as alveolar wall. Typical examples of control and damaged lung images are shown in Fig. 7 with corresponding digital masks. The segmentation process defined a parameter that numerically described the total area of alveolar space compared with alveolar wall. Since the mathematical parameter was a measure of the available alveolar space, it gave an opposing pattern of lung damage to that obtained by measuring alveolar septal thickening, and therefore these methods were inversely correlated (Spearman's $\rho = 0.002$, Fig. 6A). For example, a low mathematical algorithm score indicates a small alveolar volume and hence a large degree of alveolar thickening and distortion, such that the lowest mathematical parameters were seen at 24 h postirradiation when the damage was greatest. The mathematical algorithm provided a rapid and valid alternative for assessing radiation-induced pulmonary damage compared with physically measuring alveolar septal thickening.

The effectiveness of the mathematical algorithm in describing radiation-induced pulmonary damage was then compared with the manual four-point scale method. The assessments obtained by these two methods were also significantly correlated (Fig. 6B, Spearman's $\rho = 0.044$).

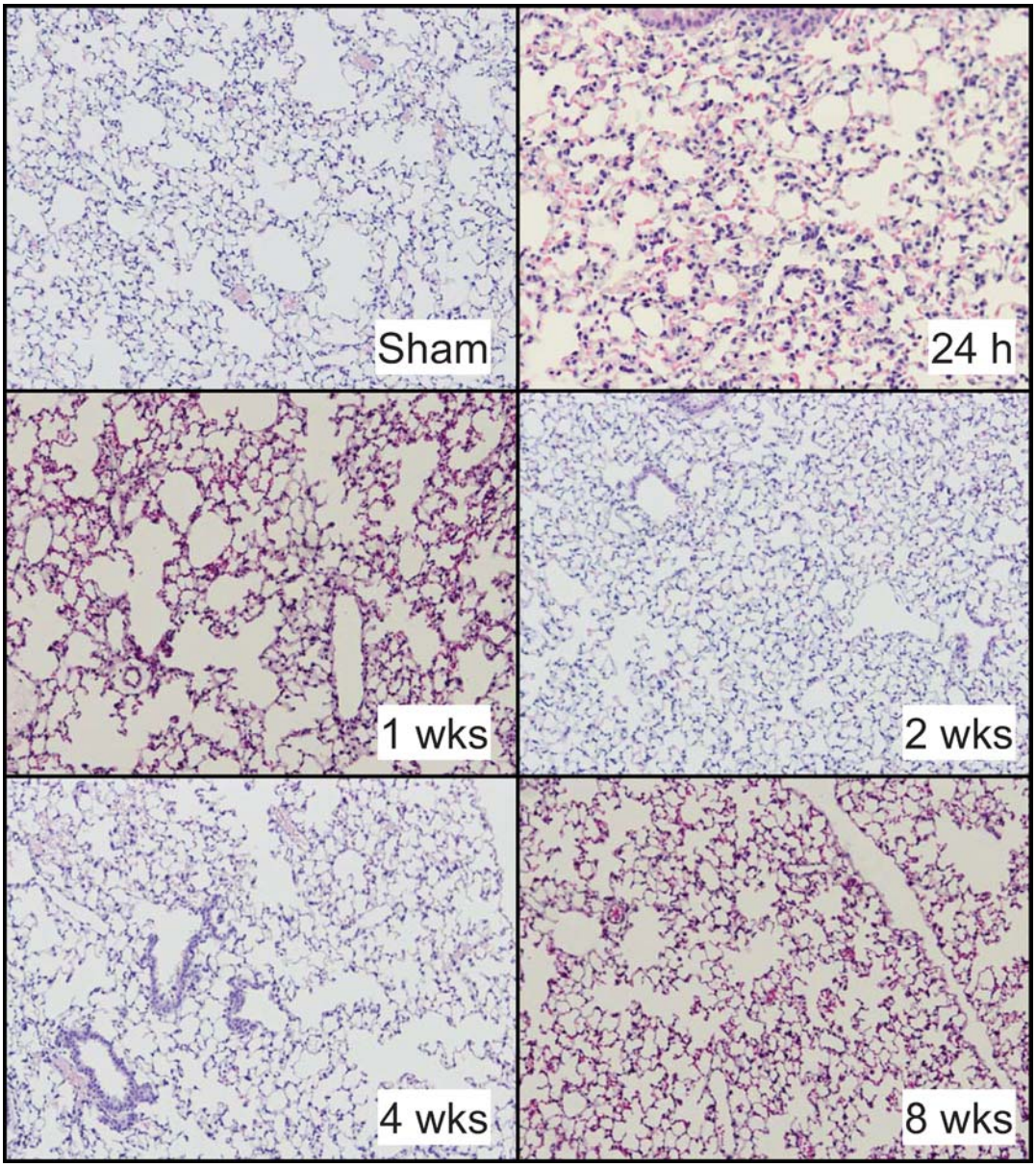

FIG. 3. H&E-stained lung sections showing representative changes in alveolar thickness with time after irradiation. The largest increases in alveolar septa can be seen at the early times after radiation exposure.

DISCUSSION

The development of lung damage after radiotherapy is a continuous process that can be attributed to radiation damage in parenchymal cells. The alveolar epithelium consists of five cell types, with the type I and type II pneumocytes widely regarded as the critical cells in radiation injury [reviewed in refs. (*13, 16*)]. The type I pneumocytes form the majority of the alveolar epithelium and are responsible for gaseous exchange. After radiation exposure the alveolar surface rapidly becomes denuded of type I pneumocytes, and type II pneumocytes are stimulated to proliferate (*17*). The acceleration in growth of type II cells is regulated by cytokines and growth factors released by macrophages, epithelial cells and type I cells and leads to the transformation of type II pneumocytes into type I alveolar epithelial cells (*5, 8, 18*). The alveolar epithelium is therefore restored rapidly. Moreover, type II pneumocytes are responsible for tissue degradation and remodeling after lung injury during the early and later stages of pulmonary fibrosis (*19*). Although alveolar macrophages are the main source of proinflammatory cytokines early after radiation exposure (*20*), the alveolar epithelium contributes to regulating the acute tissue response in an autocrine and paracrine fashion (*21, 22*). Early acute interstitial inflammation is characterized histopathologically by structural alterations to the alveolar walls and a reduction in size of the alveolar space. Infiltrations of inflammatory cells that reside in the lung, along with

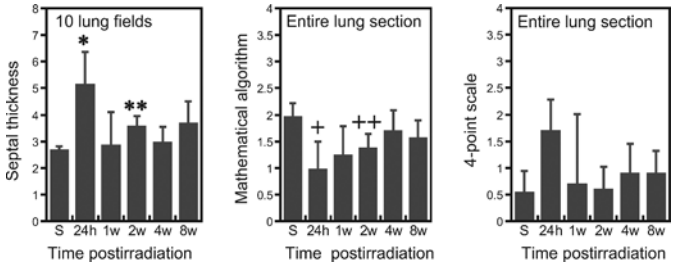

FIG. 4. A comparison of lung injury assessed using the three scoring methods. Entire lung sections were used to define the pathological score using the manual four-point scale and also using the automated mathematical algorithm. The thickness of the alveolar septa was determined from repeated measurements made in 10 randomly selected representative microscope fields. The pattern of response is qualitatively similar between the manual and measured methods since these approaches consider the alveolar septa, whereas the mathematical approach evaluates the reduction in alveolar space and consequently the pattern of response appears as the inverse of alveolar wall-based methods. */$^{+}$ signifies statistically significant differences compared with sham (S)-treated animals ($P < 0.05$, Student's T test). *$P = 0.029$; **$P = 0.003$; $^{+}P = 0.009$; $^{++}P = 0.008$.

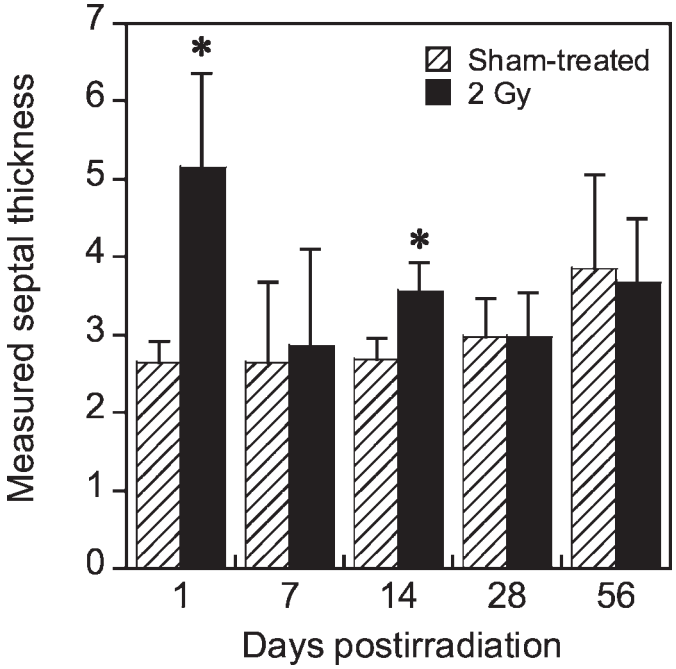

FIG. 5. Mean alveolar thickness (± SD) obtained from repeated measurements taken from 10 representative microscope fields from each animal ($n = 5$) as a function of time after X irradiation. Statistically significant differences in septal thickness were seen at 1 day (Student's t test, $P = 0.002$) and 14 days (Student's t test, $P = 0.029$) postirradiation. No significant differences were evident at 4 or 8 weeks postirradiation or between the sham-treated animals at all times.

those recruited to the lung after injury, invade the alveolar ducts and sacs and decrease the alveolar volume. After high radiation doses, the local infiltration of inflammatory cells into the pulmonary interstitium leads to destruction of the tissue architecture.

In this study the thickness of alveolar septa was found to increase significantly 24 h postirradiation, although variation was seen between the five animals in the group [mean 5.2 μM (± 1.21 μM SD)]. Significant alveolar thickening was also evident 2 weeks postirradiation, but by 4 weeks the level of damage was indistinguishable from that in sham-treated controls. Broadly similar results describing tissue remodeling with alveolar thickening at 4 and 21 days can be seen in the micrographs from the study of Tian and colleagues using the same mouse strain irradiated with a whole-body dose of 2 Gy (*23*) and in the early time radiation controls in the study of Para *et al.* (*24*), albeit after a higher radiation dose, but otherwise the images are similar considering the different techniques and times. In the current study, distinct alveolar thickening was evident only in the irradiated animals and therefore is unlikely to reflect procedural differences in the preparation of the individual samples.

The same temporal pattern of lung damage defined by measuring the physical thickness of the septa was also evident when injury was assessed using the manual four-point scale. Despite the apparent severity of these early changes in tissue architecture, no noticeable changes in animal behavior or breathing complications were observed compared with sham-treated animals. Changes in breathing rates would be expected after higher-dose exposures (*25*). Assessing radiation-induced pulmonary damage by measuring septal thickness proved to be a time-consuming process that required some expert histopathological knowledge and was prone to unintended selection bias when choosing representative fields. To overcome these limitations, we developed a simple automated image segmentation routine that examined damage across the entire lung section. Similar approaches have been used previously to measure fibrosis damage after higher doses (*26*). We demonstrated that the mathematical assessment of tissue damage was significantly correlated with the measured assessment of septal thickness (Fig. 6). The mathematical algorithm primarily assessed alveolar space, which is inversely reflective of thickening of alveolar wall, so a significant correlation between the two methods was anticipated.

We then compared the results from the mathematical assessment with a manual estimation of lung damage made using a four-point scale since this is an accepted method of damage assessment for this tissue, albeit a semiquantitative method (*13, 14*). Both these evaluation methods considered damage across the entire lung section and at the same magnification. A significant correlation was found between these two methods indicating that the mathematical method is a good surrogate measure for evaluating radiation-induced lung damage (Spearman's $\rho = 0.044$). Assessing damage using the mathematical method proved to be considerably quicker than either the septal measurement or four-

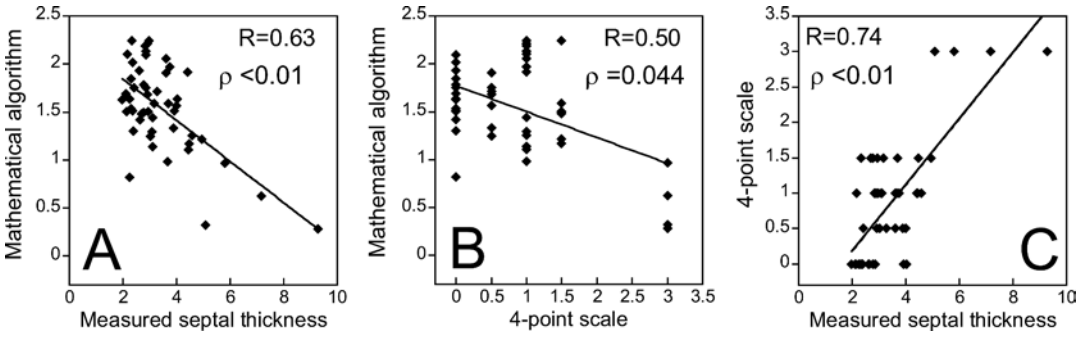

FIG. 6. Multivariate nonparametric correlation plots showing the strength of the linear relationships between the three scoring methods. The mathematical and measured methods were significantly correlated (panel A, Spearman's $\rho = 0.002$), as were the manual and measured methods (panel C, $\rho = 0.001$) and mathematical and manual scoring techniques (panel B, $\rho = 0.045$).

point scale method and was not reliant on scorer-selected images. Therefore, we consider the mathematical method to have advantages over the other two methods, the most important of which being the elimination of any scoring variability and inadvertent operator bias. Reducing scoring variability is important when damage is assessed by multiple assessors or when damage is measured over a long time. Ashcroft reported highly significant differences in mean scores recorded between five observers using a manual grading system to score lung fibrosis in the same sections and also appreciable intraobserver variability on repeated measurements of the same section (*14*). In contrast, the mathematical algorithm generates the same parameter value on each implementation. Of the three methods, the physical measurement of septal thickness was the most time consuming, with the mathematical algorithm method taking the least time.

A limitation of the mathematical algorithm is that no detailed information about the mechanism of alveoli damage is obtained, whether by septal wall thickening or the invasion of inflammatory cells in the alveolar space. Clearly, the four-point scale remains valuable since both the contributions of septal thickening and cell invasion are determined simultaneously, and this distinction can provide information about the underlying mechanism of lung damage. This would be particularly important, for example, when evaluating diffuse radiation-induced damage in combination with localized damage caused by pulmonary infections (e.g. from bacterial or fungal sources) that enter the lungs via the bronchioles and activate different damage response pathways.

No assessment of cytokine changes was made in the current study, but those experiments are ongoing. The pulmonary invasion of neutrophils, lymphocytes and macrophages was seen with increasing time postirradiation but decreased by 4 weeks (manuscript in preparation) as has been reported previously after higher-dose exposures (*5, 11*). Increased mRNA levels of IL-1β and TNF-α have been reported within 1 h postirradiation with doses as low as 1 Gy, although higher doses induced greater IL-1β gene expression (*9*). Similar patterns of pro-inflammatory cytokine expression have been reported for different mouse strains (C3H/HeJ and C57BL/6J) despite differences in late responses to pulmonary irradiation (*9*). Rübe and colleagues (*22*) reported radiation-induced TNF-α expression within 6 h in the bronchiolar epithelium, which preceded IL-1α and IL-6 expression. Since the greatest level of alveolar septal thickening in the current study was seen very early after treatment with little evidence of large numbers of infiltrating cells (24 h postirradiation) (Fig. 5), we

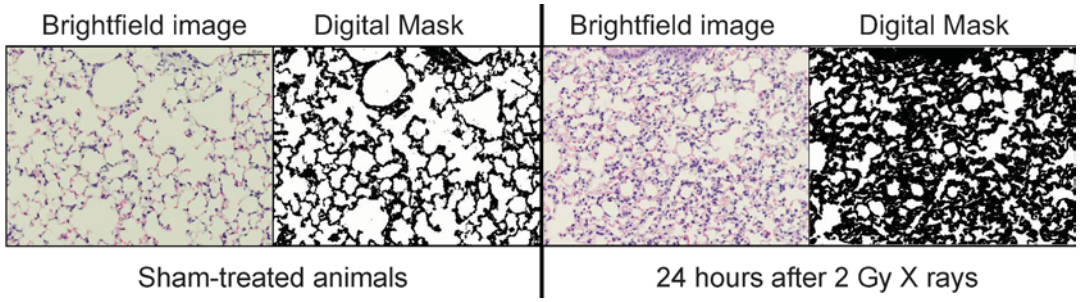

FIG. 7. H&E-stained lung sections with corresponding segmentation masks defined by the mathematical algorithm. The black and white components of the mask correspond to measures of the alveolar walls and alveolar space, respectively.

postulate that the thickening most likely reflects the release of pro-inflammatory cytokines originating from the bronchiolar epithelium rather than infiltrating cells, although our future studies may clarify this.

The conclusions from the current data are likely to extend to other mouse strains even though the C57BL/6 strain is regarded as prone to developing radiation fibrosis (*31, 32*) due to a susceptibility to radiation-induced pulmonary apoptosis (*33*). However, genetic background has been shown to influence susceptibility for perivascular inflammation and recruitment of inflammatory cells into lung tissue in models of airway inflammation (*34*), so any assessments of radiation damage using these criteria are likely to differ between strains.

For clinical studies, obtaining tissue from patients is not always feasible, so the levels of radiation-induced circulating cytokines have been used as a surrogate assay to predict radiation pneumonitis. Changes in serum levels of KL-6, a glycoprotein strongly expressed by type II alveolar pneumocytes, before and after radiotherapy have been shown to provide a better estimate of radiation pneumonitis in patients than the absolute peak value of KL-6 in the serum (*27*). A similar conclusion was reached in a smaller study of lung radiotherapy patients (*28*). In contrast, others have reported that neither the absolute nor any relative values of cytokine plasma levels identified non-small-cell lung carcinoma patients at risk of radiation pneumonitis (*21*). The elevation of plasma TGF-β1 levels 4 weeks during radiotherapy has also been shown to be significantly predictive of radiation-induced lung toxicity in patients (*29*), as has TNF-α in a murine study (*30*). In C57BL/6 mice, the expression of TNF-α 2–3 months after radiation exposure has been suggested as critical in the regulation of pneumonitis (*11*).

Overall, the data demonstrate that alveolar septal thickening, which is a characteristic of the acute inflammatory response of radiation pneumonitis, can be defined reliably by a simple calculation using a segmentation algorithm. This surrogate technique for assessing early-onset radiation-induced pulmonary injury is rapid, can be performed with any captured digital image of the lung, and is independent of operator and selection bias. We are now investigating whether this automated technique has sufficient sensitivity to measure low levels of late radiation-induced injury or injury that results from combined pulmonary injury such as would occur after a radiation exposure combined with either a bacterial or fungal infection. However, this may require a more sophisticated algorithm that considers both alveolar thickness and inflammatory cell invasion. Likewise, pulmonary damage from higher radiation doses that involve more tissue remodeling and greater inflammatory infiltration than seen in the current study may also require more sophisticated algorithms.

ACKNOWLEDGMENTS

This work was supported by Center for Biophysical Assessment and Risk Management Following Irradiation (CBARMFI, Rochester, NY), the William Beaumont Hospital Research Institute and Department of Radiation Oncology, William Beaumont Hospital. We thank Dr. Jacqueline Williams and Dr. Jacob Finkelstein (University of Rochester, NY) for continued support and encouragement of this work, and for helpful discussions. The authors wish to thank Dr. Mitual Amin for assistance and guidance with describing lung histopathology, Barbara Pruetz (Beaumont BioBank) for histopathological technical support, and Sandra Galoforo for assistance with animal irradiations.

Received: January 7, 2009; accepted: August 7, 2009; published online: January 28, 2010

REFERENCES

1. S. McDonald, P. Rubin and P. Maasilta, Response of normal lung to irradiation. Tolerance doses/tolerance volumes in pulmonary radiation syndromes. *Front. Radiat. Ther. Oncol.* **23**, 255–276; discussion 299–301 (1989).
2. N. J. Gross, Pulmonary effects of radiation therapy. *Ann. Intern. Med.* **86**, 81–92 (1977).
3. E. L. Travis, The sequence of histological changes in mouse lungs after single doses of x-rays. *Int. J. Radiat. Oncol. Biol. Phys.* **6**, 345–347 (1980).
4. J. E. Coggle, B. E. Lambert and S. R. Moores, Radiation effects in the lung. *Environ. Health Perspect.* **70**, 261–291 (1986).
5. C. J. Johnston, J. P. Williams, A. Elder, E. Hernady and J. N. Finkelstein, Inflammatory cell recruitment following thoracic irradiation. *Exp. Lung Res.* **30**, 369–382 (2004).
6. P. Rubin, J. Finkelstein and D. Shapiro, Molecular biology mechanisms in the radiation induction of pulmonary injury syndromes: interrelationship between the alveolar macrophage and the septal fibroblast. *Int. J. Radiat. Oncol. Biol. Phys.* **24**, 93–101 (1992).
7. F. M. Kong, X. Ao, L. Wang and T. S. Lawrence, The use of blood biomarkers to predict radiation lung toxicity: a potential strategy to individualize thoracic radiation therapy. *Cancer Control* **15**, 140–150 (2008).
8. P. Rubin, C. J. Johnston, J. P. Williams, S. McDonald and J. N. Finkelstein, A perpetual cascade of cytokines postirradiation leads to pulmonary fibrosis. *Int. J. Radiat. Oncol. Biol. Phys.* **33**, 99–109 (1995).
9. J. H. Hong, C. S. Chiang, C. Y. Tsao, P. Y. Lin, W. H. McBride and C. J. Wu, Rapid induction of cytokine gene expression in the lung after single and fractionated doses of radiation. *Int. J. Radiat. Biol.* **75**, 1421–1427 (1999).
10. C. J. Johnston, T. W. Wright, P. Rubin and J. N. Finkelstein, Alterations in the expression of chemokine mRNA levels in fibrosis-resistant and -sensitive mice after thoracic irradiation. *Exp. Lung Res.* **24**, 321–337 (1998).
11. C. S. Chiang, W. C. Liu, S. M. Jung, F. H. Chen, C. R. Wu, W. H. McBride, C. C. Lee and J. H. Hong, Compartmental responses after thoracic irradiation of mice: strain differences. *Int. J. Radiat. Oncol. Biol. Phys.* **62**, 862–871 (2005).
12. J. E. Craighead, J. L. Abraham, A. Churg, F. H. Green, J. Kleinerman, P. C. Pratt, T. A. Seemayer, V. Vallyathan and H. Weill, The pathology of asbestos-associated diseases of the lungs and pleural cavities: diagnostic criteria and proposed grading schema. Report of the Pneumoconiosis Committee of the College of American Pathologists and the National Institute for Occupational Safety and Health. *Arch. Pathol. Lab. Med.* **106**, 544–596 (1982).
13. S. McDonald, P. Rubin, T. L. Phillips and L. B. Marks, Injury to the lung from cancer therapy: clinical syndromes, measurable

endpoints, and potential scoring systems. *Int. J. Radiat. Oncol. Biol. Phys.* **31**, 1187–1203 (1995).

14. T. Ashcroft, J. M. Simpson and V. Timbrell, Simple method of estimating severity of pulmonary fibrosis on a numerical scale. *J. Clin. Pathol.* **41**, 467–470 (1988).
15. E. I. Stearns, *Colorimetry*, 2nd ed. *Color Res. Appl.* **13**, 64–65 (1988).
16. K. R. Trott, T. Herrmann and M. Kasper, Target cells in radiation pneumopathy. *Int. J. Radiat. Oncol. Biol. Phys.* **58**, 463–469 (2004).
17. E. L. Travis, R. A. Harley, J. O. Fenn, C. J. Klobukowski and H. B. Hargrove, Pathologic changes in the lung following single and multi-fraction irradiation. *Int. J. Radiat. Oncol. Biol. Phys.* **2**, 475–490 (1977).
18. M. Kasper and G. Haroske, Alterations in the alveolar epithelium after injury leading to pulmonary fibrosis. *Histol. Histopathol.* **11**, 463–483 (1996).
19. W. F. Ward, A. Molteni, N. H. Solliday and G. E. Jones, The relationship between endothelial dysfunction and collagen accumulation in irradiated rat lung. *Int. J. Radiat. Oncol. Biol. Phys.* **11**, 1985–1990 (1985).
20. J. N. Finkelstein, C. J. Johnston, R. Baggs and P. Rubin, Early alterations in extracellular matrix and transforming growth factor beta gene expression in mouse lung indicative of late radiation fibrosis. *Int. J. Radiat. Oncol. Biol. Phys.* **28**, 621–631 (1994).
21. C. E. Rube, J. Palm, M. Erren, J. Fleckenstein, J. Konig, K. Remberger and C. Rube, Cytokine plasma levels: reliable predictors for radiation pneumonitis? *PloS One* **3**, e2898 (2008).
22. C. E. Rübe, D. Uthe, F. Wilfert, D. Ludwig, K. Yang, J. Konig, J. Palm, A. Schuck, N. Willich and C. Rübe, The bronchiolar epithelium as a prominent source of pro-inflammatory cytokines after lung irradiation. *Int. J. Radiat. Oncol. Biol. Phys.* **61**, 1482–1492 (2005).
23. J. Tian, M. J. Pecaut, G. B. Coutrakon, J. M. Slater and D. S. Gridley, Response of extracellular matrix regulators in mouse lung after exposure to photons, protons and simulated solar particle event protons. *Radiat. Res.* **172**, 30–41 (2009).
24. A. E. Para, A. Bezjak, I. W. Yeung, J. Van Dyk and R. P. Hill, Effects of genistein following fractionated lung irradiation in mice. Effects of genistein following fractionated lung irradiation in mice. *Radiother. Oncol.* **92**, 500–510 (2009).
25. C. J. Johnston, J. P. Williams, P. Okunieff and J. N. Finkelstein, Radiation-induced pulmonary fibrosis: examination of chemokine and chemokine receptor families. *Radiat. Res.* **157**, 256–265 (2002).
26. R. Kraus, F. Steinberg, B. Rehn, J. Bruch and C. Streffer, Radiation-induced changes in lung tissue and development of fibrosis determined by quantitative morphometric methods. *J. Cancer Res. Clin. Oncol.* **117**, 27–32 (1991).
27. R. Tokiya, J. Hiratsuka, K. Yoshida, S. Imai, Y. Kajihara and Y. Imajo, Evaluation of serum KL-6 as a predictive marker of radiation pneumonitis in patients with breast-conservation therapy. *Int. J. Clin. Oncol./Jpn. Soc. Clin. Oncol.* **9**, 498–502 (2004).
28. R. Hara, J. Itami, T. Komiyama, D. Katoh and T. Kondo, Serum levels of KL-6 for predicting the occurrence of radiation pneumonitis after stereotactic radiotherapy for lung tumors. *Chest* **125**, 340–344 (2004).
29. L. Zhao, K. Sheldon, M. Chen, M. S. Yin, J. A. Hayman, G. P. Kalemkerian, D. Arenberg, S. E. Lyons, J. L. Curtis and F. M. Kong, The predictive role of plasma TGF-beta1 during radiation therapy for radiation-induced lung toxicity deserves further study in patients with non-small cell lung cancer. *Lung Cancer* **59**, 232–239 (2008).
30. M. Zhang, J. Qian, X. Xing, F. M. Kong, L. Zhao, M. Chen and T. S. Lawrence, Inhibition of the tumor necrosis factor-alpha pathway is radioprotective for the lung. *Clin. Cancer Res.* **14**, 1868–1876 (2008).
31. C. K. Haston and E. L. Travis, Murine susceptibility to radiation-induced pulmonary fibrosis is influenced by a genetic factor implicated in susceptibility to bleomycin-induced pulmonary fibrosis. *Cancer Res.* **57**, 5286–5291 (1997).
32. J. P. Williams, E. Hernady, C. J. Johnston, C. M. Reed, B. Fenton, P. Okunieff and J. N. Finkelstein, Effect of administration of lovastatin on the development of late pulmonary effects after whole-lung irradiation in a murine model. *Radiat. Res.* **161**, 560–567 (2004).
33. T. J. O'Brien, S. Letuve and C. K. Haston, Radiation-induced strain differences in mouse alveolar inflammatory cell apoptosis. *Can. J. Physiol. Pharmacol.* **83**, 117–122 (2005).
34. B. Singh, K. Shinagawa, C. Taube, E. W. Gelfand and R. Pabst, Strain-specific differences in perivascular inflammation in lungs in two murine models of allergic airway inflammation. *Clin. Exp. Immunol.* **141**, 223–229 (2005).